Dimpling process in cold roll metal forming by finite element modelling and experimental validation

V B Nguyen, Chang Wang, D J Mynors, M A English, M A Castellucci

Publication date
01-08-2014

Document Version
Accepted version

Published in
Journal of Manufacturing Processes

Link to external publisher version
https://doi.org/10.1016/j.jmapro.2014.03.001

Dimpling process in cold roll metal forming by finite element modelling and experimental validation

V.B. Nguyen[a,c,*], C.J. Wang[a], D.J. Mynors[b], M.A. English[c], M.A. Castellucci[c]

[a] *Department of Engineering and Technology, University of Wolverhampton, Telford Campus, Telford, TF2 9NT, United Kingdom*

[b] *School of Engineering and Informatics, University of Sussex, Sussex House, Brighton, BN1 9RH, United Kingdom*

[c] *Hadley Industries plc, PO Box 92, Downing Street, Smethwick, West Midlands, B66 2PA, United Kingdom*

[*] Corresponding author.

Hadley Industries plc, PO Box 92, Downing Street, Smethwick, West Midlands, B66 2PA, United Kingdom

Tel: +44 121 555 1330; fax: +44 121 555 1331.

Email: bac.nguyen@hadleygroup.co.uk (V.B. Nguyen)

Keywords: Cold-rolled, dimpling process, finite element modelling, plastic strain, mechanical testing

Abstract

The dimpling process is a novel cold-roll forming process that involves dimpling of a rolled flat strip prior to the roll forming operation. This is a process undertaken to enhance the material properties and subsequent products' structural performance while maintaining a minimum strip thickness. In order to understand the complex and interrelated nonlinear changes in contact, geometry and material properties that occur in the process, it is necessary to accurately simulate the process and validate through physical tests. In this paper, 3D non-linear finite element analysis was employed to simulate the dimpling process and mechanical testing of the subsequent dimpled sheets, in which the dimple geometry and material properties data were directly transferred from the dimpling process. Physical measurements, tensile and bending tests on dimpled sheet steel were conducted to evaluate the simulation results. Simulation of the dimpling process identified the amount of non-uniform plastic strain introduced and the manner in which this was distributed through the sheet. The plastic strain resulted in strain hardening which could correlate to the increase in the strength of the dimpled steel when compared to plain steel originating from the same coil material. A parametric study revealed that the amount of plastic strain depends upon on the process parameters such as friction and overlapping gap between the two forming rolls. The results derived from simulations of the tensile and bending tests were in good agreement with the experimental ones. The validation indicates that the finite element analysis was able to successfully simulate the dimpling process and mechanical properties of the subsequent dimpled steel products.

1. Introduction

The cold roll forming process is the progressive forming of steel strip into a desired section by passing through a series of rolls, arranged in tandem. It is generally the most economic method of manufacturing sections. The optimum economic viability in manufacturing industry requires a minimisation of the amount of material used while the structural performance of roll-formed products relies on maintaining the stiffness and strength of the section. Additional bends introduced into the section such as 'intermediate stiffeners' can be a solution for these conflicting requirements. They have been found to improve the material properties of the finished product as the yield and tensile strength of the material increases within the deformed zone around the bends; however, such improvements are limited [1,2]. An alternative mechanism to improve the material and structural performance is to impart a deformation to the whole sheet. The UltraSTEEL® process or dimpling process, developed by Hadley Industries plc is an industrial manufacturing process which achieves this deformation. The process uses a pair of rolls which are designed with rows of specially shaped teeth that deform the strip creating the dimple shapes from both sides of the plain sheet prior to the traditional cold roll forming process [3], as shown in Fig. 1. Dimpled steel products are increasingly used in a wide range of applications, including wall studs, framing and roofing members, corrugated panels, vineyard posts, windows and door reinforcement and many other products.

- Allocation of **Fig. 1**

Fig. 1. The UltraSTEEL® process and dimpled steel sheet (Courtesy of Hadley Industries plc).

The effect of the dimpling process on the mechanical and structural properties of the steel material has been the subject of some recent experimental investigations through micro-hardness, tensile, bending and compression tests of plain and dimpled steel specimens [3-7]. The tests revealed that the strength of dimpled specimens was significantly greater than plain specimens originating from the same coil material, and this enhancement is a result of the cold work applied to the material during the dimpling process.

Besides experimental tests, numerical models have been conducted to study the plastic strain induced during the dimpling process in order to understand the mechanism of the dimpling process. An initial review of the numerical models for the dimpling process has been presented in Nguyen et al [9]. Some are presented here again together with the latest investigation. Hartley and Pillinger [8] introduced one of the first numerical models for the dimpling process in which an elastic-plastic model was used within the finite element analysis. In this investigation, only one dimple was formed by spherical indenters that centred at each corner of a square steel plate and translated normally to the plate surface. It was found that plastic strain developed throughout the plate, and higher plastic strain was generated at the plate surface on the opposite side to the intender. Despite illustrating some important features of the dimpling process, this model was not able to predict accurately the amount of plastic strain induced during the dimpling process because in the actual process, each indenter (tooth) has a more complex geometry and contacts the plate via a rotational movement on the periphery of a roll. A finite element model of the dimpling process was later developed by Wang et al. [10] in which rotating rolls rotating rolls deformed the flat strip into dimpled strip via their teeth which had correct geometry. The plastic strain developed in the dimples together with the effect of rolling setup, were studied. However, these models have not been fully calibrated on the basis of physical measurements of the process

and the mechanical properties of dimpled sheet. In addition, the dimpling process involves the complex and interrelated nonlinear changes in contact, geometry and material properties of the dimpled steel sheet. Recently, Nguyen et al. [9] proposed a practical finite element approach of modelling the dimpling process and subsequent dimpled products. In this approach, a simplified process was developed in which the top and bottom rolls were translated vertically to deform a square plate into a dimple. This generic dimple geometry was used to generate dimpled products- if it was a very large dimpled product then shell elements were used instead of three dimensional (3D) elements. Only the geometry of the dimple was transferred from the dimpling process, the material properties of the dimple were given from a separate tensile test on a dimpled steel sample. It has been approved that this simplified model was a powerful method to practically represent large dimpled products as the model significantly reduced number of elements used that saved computational costs. In this approach, residual stresses and plastic strain developed during the dimpling process were not included in the simulations as there is no method available to incorporate these data for dimpled steel. The simplified approach in Nguyen et al. [9] was used to practically represent dimpled products in cold forming processes. This approach can be summarised as following steps: (1) simulating a simplified dimpling process that deform a flat steel plate into a dimple, (2) use this generic dimple geometry to generate dimpled strip- if it is a very large dimpled product then shell element approach instead of 3D element approach is applied instead. It should be noted that only the geometry of the dimple is transferred from the dimpling process in step (1), material properties of the dimple is given from a separate tensile test on a dimpled steel sample, (3) simulating the cold forming process that develop the dimpled strip into a desired dimpled product (4) simulating the dimpled products subject to mechanical tests (for example, under tension, bending or compression tests). However, it would be ideal to

simulate the actual dimpling process and retain the resultant data, i.e. stress and strain data, of the dimpled sheet from the previous dimpling process simulation. Hence, both the dimpled sheet geometry and material properties generated from the dimpling process are used in the next simulations including mechanical testing on the dimpled sheet. The plastic strains and residual stresses, thus, would be retained in the dimpled steel material; this allows gaining insight into the dimpling process and its effects on the mechanical properties of the dimpled steel, and thereby optimising the process.

In this paper, Finite Element (FE) modelling of the actual dimpling process was first developed. In this simulation, a long flat steel sheet was transported through a pair of rotating rolls and deformed into a dimpled steel sheet. The dimpled steel sheet was then subjected to tension and bending, in which the dimple geometry and material properties data were directly transferred from the dimpling process. The plastic strains and residual stresses are retained in the dimpled steel material which allowed the mechanical and structural properties of the dimpled steel to be assessed accurately. Physical measurements and mechanical tests were initially conducted on dimpled steel sheets [9] and the experimental results were compared with the FE results. The end purposes of performing mechanical tests and FE simulations including tension and bending on the dimpled sheet were to evaluate the FE simulation of the dimpling process. Simulations of plain steel sheet under mechanical testing were carried out in parallel with dimpled sheet in order to assess the effects of the dimpling process and to further evaluate the FE results. Furthermore, different values of process parameters including friction and tooth overlapping gap were used in modelling to investigate the effects of process parameters on the work hardening of the dimpled sheet and its structural capacity.

The ideal approach is used in this paper to accurately simulate the whole manufacturing processes starting from a plain steel strip to the final dimpled products subject to mechanical tests in consecutive steps: (1) simulating an actual dimpling process i.e. rotating rolls, that deforms a flat steel strip into a dimpled strip, (2) use the subsequent dimpled strip (generated from the first dimpling process) as a desire dimpled product in which the geometry of the dimpled strip together with its material data including stress/strain data generated from the dimpling process - step (1) are directly transferred to the next loading step simulation, and (3) simulating the dimpled products subject to mechanical tests (for example, under tension and bending tests). The new approach presented in this paper can gain insight into the dimpling process and its effects on the mechanical and structural properties of dimpled steel products, and hence to optimize the process later in the future.

2. Finite Element modelling

Finite Element simulations were conducted using Marc (MSC Software Corporation, version 2011) to simulate the dimpling process and mechanical tests of dimpled sheets. The simulations were carried out in two stages: (1) the dimpling process was simulated first, and (2) tension and bending of the subsequent dimpled sheet were simulated, in which the dimple sheet's resultant geometry and stress/strain data were directly transferred from the dimpling process using the PRE STATE procedure in Marc. Small mesh sizes and 3D solid elements were used in order to well capture the complicated bending and stretching behaviour of the dimpled sheet, so the geometric details of the dimple were modelled.

A parametric study was carried out to investigate the effects of several modelling parameters on the reliability of the FE model and results. Based on this investigation, a set of appropriate parameters were selected as follows:

i. Mesh density: two different meshes, MESH I and MESH II, illustrated in Fig. 2, were used for the plain strip. MESH I had 37,980 solid elements of 0.178 mm × 0.355 mm × 0.347 mm, and MESH II was a very fine mesh, of 149,810 elements of 0.178 mm × 0.178 mm × 0.176 mm. The dimpling simulation revealed that the maximum plastic strain and stress developed in MESH I differed from those of MESH II by less than 7% and 4%, respectively. Therefore, MESH I was considered accurate enough to be used in this study.

ii. Element type: 3D, eight-node, first-order, isoparametric elements with eight-point Gauss integration scheme were used (element type 7). An assumed strain procedure was used in order to improve the shear characteristics of this element.

iii. Loading step: an initial fraction of loading time of 0.001 s and a maximum fraction of loading time of 0.005 s were used for the solution to be stable and reliable. The time step was selected through a trial and error procedure by continuously reducing the time step until similar results were obtained. In particular, the first analysis started with a maximum time step of 0.02 s and then it reduced time step to a smaller one until a time step of 0.002 s. The amount of time step in one reduction varied from 0.0005 s up to 0.05 s selected based on comparing the result of the second analysis to the first analysis's. The compared results were the maximum plastic strain for the dimpling process simulation, and the ultimate forces in the tensile and bending simulations of the resultant dimpled sheets. The maximum difference in plastic strain was set up within 10% and the maximum difference in ultimate forces was set up within 5%. It was found that converged results were observed when time step was small enough, and the same results were obtained for

the analysis with a time step of 0.005 s and 0.002 s. Therefore, a maximum time step of 0.005 s was selected in this study. It should be noted that this time step was selected in association with a reasonable finite element mesh (refer to 2.i.), an implicit analysis type with a full iteration method (refer to 2.v.), and a strict convergence tolerance (force tolerance of 0.05 and displacement tolerance of 0.05, refer to 2.iv.). The convergence and consistency of the numerical results seem to justify such time step. Excellent agreements when comparing with experimental results from the tensile and bending tests especially with standard plain steel further validated this time step selection.

iv. Analysis tolerance: a relative force tolerance of 0.05 and a relative displacement tolerance of 0.05 were used for the solution to be reliable.

v. Analysis type: an implicit, static analysis was employed. A full Newton-Raphson method was used for the iterative procedure.

- Allocation of **Fig. 2**

Fig. 2. Meshes for studying mesh density (a) MESH I, and (b) MESH II.

2.1. FE simulation of the UltraSTEEL® process

CAD models of the top and bottom UltraSTEEL® rolls were imported into Marc for pre-processing. The plain strip of 75 mm in length, 12.50 mm in width and 0.90 mm in gauge thickness was generated in Marc and placed in a pre-defined position between the two rolls. Based on the dimensions of the plain strip, only quarters of the rolls were modelled, as shown in Fig. 3.

- Allocation of **Fig. 3**

Fig. 3. 3D view of the FE model: (a) whole model, and (b) detailed view of the roll teeth and plain sheet together with their meshes.

The top and bottom rolls were modelled as rigid bodies, which rotated about their central axes. The steel strip was modelled as a deformable body with 37,980 solid elements; they were 3D, eight-node, hexahedral elements. The minimum element size in the model was 0.17 mm; it was small enough to model the curved geometry of the dimples. Five layers of elements were used through the strip thickness to capture both bending and stretching phenomena that occur during the process. The contact between the roll teeth and the steel strip was modelled as contact surfaces using 3D contact elements. The friction between the steel strip and the teeth was assumed isotropic and modelled by Coulomb's law with a friction constant of 0.30. Coulomb friction model was chosen following a vast of studies in literature have also used this model for cold roll forming simulations. The Coulomb friction model thus was mainly used in this study as a demonstration on the effect of friction on the plastic distribution of the dimpling process. It is not within the scope of this study to investigate different friction models. However, friction measurements and different friction models for the dimpling process will be investigated in the future work. The value of 0.3 for the friction coefficient was not validated against physical measurements as physical data for friction was not available. Generally, measuring friction coefficient is very difficult as it varies in time and space with many parameters such as roll geometry, sliding velocity, lubrication conditions, and contact pressure. As the dimpling process produces a strip with a complex 'dimpled' surface topography there are no existing methods to determine friction during the dimpling process in particular. Therefore no physical data for

friction was available for direct comparison with the value of 0.3 used in this study. However, this value was chosen based on a sensitivity analysis to the friction coefficient as described in details in the paper, and also referred to values suggested in literature, i.e. Wang et al. [10]. In addition, if the consistency of results could be obtained (for tensile and bending test simulations in comparison with tests) it could seem to further justify such assumption.

The top and bottom rolls had an overlapping gap of 0.40 mm between the mating teeth and were rotated about z-z axis at an angular velocity ω clockwise and anti-clockwise, respectively. The sheet was fully fixed at one end (on the right side, in Fig. 3(a)) and initially fed to the rotating rolls with a velocity equal to the linear velocity at the tip of the roll teeth. When the roll teeth just grasped the strip surfaces, the fixed end was released from the fully fixed condition and the strip was freely deformed by the rotating rolls.

The displacement imparted on the steel strip during the dimpling process and in mechanical testing was large. Therefore, large strain model was applied in order to take into account the geometric and material nonlinearity that occurred. An elastic-plastic material model with strain hardening using Von Mises yield criterion was used for the sheet steel to model the material nonlinearity. The material has a Young's modulus of 205 GPa and a Poisson's ratio of 0.30. Material properties of the plain steel strip were obtained from the tensile tests, in the form of the engineering stress and strain data as shown in Fig. 4. In FE simulations, the material stress and strain data required to be input in the form of the true stress (σ_{true}) and true plastic strain (ε^{p}_{true}). Therefore, the true stress and true plastic strain were converted from the engineering stress (σ_{nom}) and engineering strain (ε_{nom}) as follows:

$$\sigma_{true} = \sigma_{nom}(1 + \varepsilon_{nom}) \quad (1)$$

$$\varepsilon^{p}_{true} = \ln(1 + \varepsilon_{nom}) - \sigma_{nom}/E \quad (2)$$

- Allocation of **Fig. 4**

Fig. 4. Engineering stress-strain curve of the plain steel material

The dimpling process simulation was required to use material data for the plain steel sheet. This material data was obtained from a standard tensile test, presented in terms of engineering stress-strain data, as shown in Fig. 4. This engineering stress-strain data was converted to true stress-strain data, as shown in Eqns. (1) and (2), which was used in all the simulations. The maximum true strain obtained from the engineering stress-strain tensile test was about 23%. In the dimpling process simulation (and subsequent mechanical test simulations), when strain went beyond the maximum true strain obtained from tensile test, it was extrapolated based on the last slope in the data. In the tensile test and bending test simulations, the original true stress-strain data were used together with stress-strain data transferred from the previous dimpling process simulation (stress-strain data at the end of the dimpling process). The dimpled sheet geometry was used and PRE STATE procedure in Marc was employed to directly transfer resultant stress and strain data from the previous dimpling process simulation (pre-state) into the new simulation as an initial state. The current plastic strain of the new simulation (tension or bending) was the plastic strain during pre-state plus any additional plastic strain due to tension and/or bending. The current calculation of incremental plastic strain was based on the integration points current values including the pre-state values.

The tooth overlapping gap, $\delta = 0.40$ mm, and friction coefficient, $\mu = 0.30$, were adopted in this paper. To investigate the effects of these process parameters on the work hardening, different values of friction coefficient and tooth overlapping gap were used. Table 1 shows different

analyses in which, Analysis no. 1 is the analysis studied in this paper and was used as a reference whilst Analysis no. 2 and 3 had different values in friction and overlapping gap, respectively.

Table 1

Analyses with different values of process parameters. Shadowed numbers indicate different values to those in the reference analysis.

- Allocation of **Table 1**

2.2. FE simulation of tensile test

The original plain sheet and the dimpled sheet generated by the dimpling process were used in tension simulations. The dimpled sheet was merged into the new model in Marc in order to start the tensile analysis and PRE STATE procedure was employed to directly transfer resultant stress and strain data from the previous dimpling process simulation into the tensile simulation as an initial state. The plain/dimpled sheet had dimensions equivalent to the parallel part of the physical tensile specimen. One end of the sheet was fixed and a small incremental displacement was applied at the other end to axially stretch the strip to failure.

2.3. FE simulation of the bending test

The original plain sheet and the dimpled sheet generated by the dimpling process were used in bending simulations. The dimpled sheet was merged into the new model in Marc in order to start the bending analysis and PRE STATE procedure was employed to directly transfer resultant

stress and strain data from the previous dimpling process analysis into the bending simulation as an initial state. Top and bottom rollers were modelled as rigid bodies, in which the bottom rollers were fixed while the top roller moved down vertically to bend the sheet. The steel sheets were modelled as deformable bodies. The contact between the roll teeth and the steel strip was modelled as contact surfaces using 3D contact elements. Coulomb's law with a constant coefficient of 0.30 was used to model the friction between the steel strips and the rollers.

3. Experimental investigation

The experimental tests include the measurements of the actual UltraSTEEL® process, tensile and bending tests on the plain and dimpled steel sheets. They were presented in great detail in Nguyen et al. [9] and the results were summarised in this paper.

3.1. The UltraSTEEL® process

Steel plain strips were prepared from commercial grade galvanised steel coil, and dimpled sheets were produced by the UltraSTEEL® process. Scanned and microscope images of cross sections across the dimple peaks were used to measure the dimple dimensions and thicknesses. It has been proven that there is a direct relationship between hardness and strain in cold formed parts [11]. Therefore, the micro-hardness tests data through the thickness of the dimpled strip obtained by Collins et al. [4] were used to evaluate the pattern of plastic strain data developed in the dimpled strip during the dimpling process.

3.2. Tensile test

The plain and dimpled specimens had the ‘dog bone’ shape with an overall length of 200 mm, a parallel length of 75 mm and a width of 12.50 mm of the parallel length, and the nominal thickness of the plain specimens was 0.90 mm; they were prepared according to the British Standard, BS EN 10002-1:2001 [12]. Specimens were tested to failure at a speed of 2.50 mm/min. Three cross sectional areas along the dimpled specimen were measured using a microscope. The resulting force-extension curves were plotted. Details of the tensile test procedure and area measurements are described in Nguyen et al. [3].

3.3. Bending test

Both the plain and dimpled sheet steel specimens were produced from the same steel coil as the tensile tests and tests were carried out in compliance with the British Standard, BS 1639:1964 [13]. The specimens were rectangular with nominal length, width and thickness of 12.50 mm, 75 mm and 0.90 mm, respectively. The specimens were placed on two 4-mm diameter roller supports set at 65 mm apart, while a third top roller of 4 mm diameter was lowered onto the centre of the plate to bend the specimens. The test arrangement and a photograph of the setup are shown in Fig. 5. The load was applied through the top roller at a constant rate of 2.50 mm/min.

- Allocation of **Fig. 5**

Fig. 5. Three-point plate bending tests (a) schematic diagram, and (b) photograph of the actual test arrangement of a dimpled specimen

4. Results and discussion

4.1. The UltraSTEEL® process

Fig. 6 shows the dimpled steel sheet which was generated by the dimpling process. The deformed mesh and distribution of plastic strain throughout the dimpled sheet are also illustrated. Plastic strain was found to be non-uniform around the dimples and through the sheet thickness. It was initiated and increased around the tooth contact sites (the light shaded regions with central dark indicate the surfaces in contact with the teeth) and there was a 'cap' of higher plastic strain at the sheet surface on the opposite side to the tooth (the light shaded regions indicate the surfaces on the opposite side to the teeth). This is evidently the region in which the greatest strain hardening occurs.

- Allocation of **Fig. 6**

Fig. 6. FE dimpled strip and plastic strain distribution (a) complete dimpled sheet, and (b) detailed view of dimples and meshes.

The thicknesses of the simulated dimple sheet measured at different locations along the dimple were compared with those of the actual UltraSTEEL® sample. The shape of the predicted dimple on a plane cutting through the dimple peaks is shown in Fig. 7, in which the distribution of plastic strain is also illustrated. The numerical values at the dimple peak and slope were 0.77 mm and 0.90 mm, respectively. Fig.8 shows a microscope image of a cross section across the dimple peaks, and the measured thicknesses at the dimple peak and slope were 0.757 mm and

0.894 mm, respectively. The thickness of the predicted dimpled sheet differs from the actual process by less than 1.7% which is small.

- Allocation of **Fig. 7**

Fig. 7. Simulated dimple and plastic strain distribution. The regions of sections across the peak, valley and mid-centre line were labelled as Site 2, Site 1 and Mid-centre.

- Allocation of **Fig. 8**

Fig. 8. Microscope image of the dimple cross section

- Allocation of **Fig. 9**

Fig. 9. Plan view of (a) the simulated dimpled sheet, and (b) scanned image of the actual dimpled sheet

The plan views of the simulated dimpled sheet and scanned image of the actual dimpled sheet are shown in Fig. 9, in which measured distances between two adjacent dimple peaks in the horizontal direction (d1), vertical direction (d2), and diagonal (45^0) direction were also illustrated. Differences in d1, d2 and d3 between the simulated and actual dimpled sheets were about 3%, 2%, and 2%, respectively. This indicates that the distances of the two adjacent dimples of the simulated dimpled sheet are similar to those of the actual dimpled sheet.

The FE plastic strain pattern was further verified through comparison with micro-hardness tests [4]. Micro-hardness test results were used as an indicator to generally validate the level of plastic strain distribution from FE simulation; however, micro-hardness test results were not used

to determine a specific level of plastic strain. This comparison was only used as one amongst several validation sources to justify the process simulation results such as physically geometric measurements, tensile and bending tests. Low load micro-hardness tests were carried out and the hardness of the mid-thickness regions of the dimple (Mid-centre), and through the thickness of the dimple at the slope and peak regions (Site 1 and Site 2, respectively) are shown in Fig. 10. The micro-hardness test results used were the typical results from many measurements done in Collins et al. [4]. The FE plastic strain distribution (Fig. 7) correlated well with the micro-hardness results: for mid-centre regions (Fig. 10(a)), highest values were found on regions corresponding to the dimple slope; for Site 1 regions (Fig. 10(b)), plastic strain was raised mid centre while for Site 2 regions (Fig. 10(c)), region of highest strain was located on the sheet surface (on the opposite side to the tooth). The plastic strain distribution is generally similar to what has been observed when using the simplified model as presented in Nguyen et al. [9]. However, the plastic strain induced by this actual dimpling process is not symmetrically distributed around the dimple, as illustrated in Fig. 7, and it was mainly a result of the rotational movement of the rolls. This indicates that the model presented here is more realistic than the simplified model.

- Allocation of **Fig. 10**

Fig. 10. Micro-hardness results (a) Mid-centre region, (b) Site 1, slope region and (c) Site 2, peak region.

4.2. Tensile test

The dimple geometry and plastic strain distribution of the dimpled steel sheet before and after tension are shown in Fig. 11. The material properties of the dimpled sheet including plastic strains and residual stresses were obtained by directly transferring data from the previous dimpling simulation into the tensile simulation. Therefore, the plastic strain distribution before stretching as shown in Fig. 11(a) is similar to that at the end of the dimpling process as shown in Fig. 6(a). The dimpled sheet failed at 16% strain which is near an average of 18% strain in the test.

- Allocation of **Fig. 11**

Fig. 11. Dimple geometry and plastic strain distribution of the tensile test (a) before stretching, and (b) at breaking point.

Fig. 12 shows FE force-extension curves of plain and dimpled sheets, in which the typical force-extension curves from the test were also presented. The predicted yield and ultimate forces in the plain sheet were 2% and 4% greater than the experimental results, respectively; the predicted yield and ultimate force in the dimpled sheet were about 1% and 9% less than the experimental ones, respectively. The greater ultimate force in tests could be attributed to the fact that the actual dimpled sheet was cut from a large dimpled sheet; therefore, their edges were stiffer and had greater amount of work hardening than those in the simulated dimpled sheet where they were simulated as free edges (see Fig. 6). In addition, the difference in the ultimate forces between the tensile simulations and tests could be due to several factors used in the simulation that were not accurately known from the dimpling process such as the process speed, and actual friction between the two rolls. The tensile simulation of the dimpled sheet was stopped at an

extension of 6 mm (about 16% strain) due to non-convergent problems in the FE analysis. However, the behaviour predicted by the simulation is in good agreement with the experimental ones, especially for the plain sheet.

An elastic-plastic material model with strain hardening using Von Mises yield criterion was used in the paper (as mentioned in 2.1). Using this model and the stress-strain curve obtained from test, the breaking point in the tensile test simulation was determined as the point where the elements in the central region were largely strained and there was a sharp decrease in load-carrying capacity. The breaking point of the plain sheet specimen was captured accurately for the tensile test simulation, as shown in Fig. 12. However, the breaking point of the dimpled sheet specimen was not clearly captured as the dimpled steel was less ductile than the plain steel due to the cold work applied during the dimpling process; as a result there was no sharp decrease in the central region of the specimen and in load-carrying capacity. In this study, the breaking point of the dimpled sheet specimen was determined as the point of analysis failure (the end of the load-extension curve), as shown in Fig. 12.

- Allocation of **Fig. 12**

Fig. 12. FE and experimental force-extension curves of the plain and dimpled sheet specimens. The box shows the force-extension curves up to an extension of 1 mm. ‘EXP’ stands for ‘experimental results’ whilst ‘FE’ stands for ‘finite element results’.

In detail, the dimpled sheet steel has a higher yield and loading capacity but less ductility than the plain steel. The lack of a yield plateau in the case of dimpled sheet steel is the result of the strain hardening generated during the dimpling process. The dimpled sheet has lower stiffness

which is the slope of initial linear curve, as shown in the box in Fig. 12 for the force-extension curves up to an extension of 1 mm. This was attributed to the dimple shapes which are unfolding at the initial stages of the tensile test. The work of fracture of plain and dimpled steel was interpreted as the areas under the force-extension curves in Fig. 12. The amount of cold work exerted on the dimpled steel sheet was determined from the difference between work of fracture of plain and dimpled steel. The effect of the dimpled shape on the mechanical properties was determined based on the difference in stiffness between the force-extension curves of the plain and dimpled steel, as shown in Fig. 12. However, it was found to be very small, in comparison with the amount of the cold work, i.e. less than 1%.

4.3. Bending test

FE load-displacement curves of plain and dimpled sheets are illustrated in Fig. 13, which also shows typical load-displacement curves from the test. The FE and experimental values for ultimate load were close, with a maximum difference of 0.4% and 4% for the plain and dimpled sheets, respectively. It shows in Fig. 13 that there is an increase in the maximum force for the dimpled plate in comparison to the plain one. As the slope of the initial part of the force-displacement curves is proportional to the bending stiffness, it shows the dimpled sheet has a similar bending stiffness as the plain sheet.

- Allocation of **Fig. 13**

Fig. 13. FE and experimental force-displacement curves of the plain and dimpled sheet specimens. ‘EXP’ stands for ‘experimental results’ whilst ‘FE’ stands for ‘finite element results’.

4.4. Effects of process parameters

Fig. 14 shows plastic strain distributions on a plane cutting along the rolling direction in the three analyses demonstrating effects of process parameters including friction and tooth overlapping gap on the work hardening. The small box illustrates the strain develops at a material point, in the region in which the greatest strain hardening will occur, during the dimpling process. The effects of process parameters on the work hardening and structural performance of the dimpled sheet are shown in Table 2. In which, the maximum plastic strain developed by the dimpling process and the maximum load of the dimpled sheet predicted from bending simulation were presented.

Table 2

Maximum plastic strains introduced by the dimpling process, maximum tensile and maximum bending loads of Analysis 1, 2 and 3.

- Allocation of **Table 2**

The results confirmed that greater plastic strains were introduced in the case of greater friction between the two rolls. However, there was no significant influence of friction on the work hardening formation of the dimpled sheet. In particular, the maximum plastic strains were differed by less than 5% between friction coefficients of 0.15 and 0.30 which is small, as shown in Figs. 14(a) and (b). Furthermore, the difference was less than 10% between friction coefficients of zero and 0.30 (results not shown). The reason could be the friction at the tooth-

sheet interface appeared in the dimpling process to be mainly used to transmit the driving force from the rotating rolls to the sheet. This observation agrees with numerical studies of Bui and Ponthot [14]. This small increase in plastic strain could correlate to a small increase in the bending capacity of the dimpled sheet: about 5% increase when the friction coefficient changed from 0.15 to 0.30.

The overlapping gap had a profound effect on the work hardening formation of the dimpled sheet. When the overlapping gap increased from 0.00 mm to 0.40 mm, the maximum plastic strain increased by 18%, and plastic strain was developed in a broader region of the whole sheet, as shown in Figs. 14(a) and (c). This correlated to a significant increase of 7% in the bending capacity of the dimpled sheet.

- Allocation of **Fig. 14**

Fig. 14. Plastic strain distribution on a cutting plane along the rolling direction: (a) Analysis no. 1, (b) Analysis no. 2 and (c) Analysis no. 3. The small box illustrates the strain develops at a material point, in the region in that the greatest strain hardening will occur, during the dimpling process.

5. Conclusion

FE modelling of the UltraSTEEL® dimpling process and effects of the process parameters on the mechanical properties of dimpled steel was presented. In particular, simulations of the dimpling process and mechanical tests including tensile and bending of dimpled steel sheets were conducted. FE modelling details that related to the model setup, mesh and element type, analysis

type and control, and transferring data were described. Physical measurements, tensile and bending tests of cold-roll formed plain and dimpled steel sheets were carried out to evaluate the performance of the FE simulations.

The simulation of the UltraSTEEL® dimpling process illustrated that during the dimpling process, various levels of non-uniformed plastic strain were developed throughout the thickness of the steel sheet. These observations agreed well with experimental measurements including micro-hardness test, scanned and microscope images.

The results of tensile and bending simulations of plain and dimpled sheets were in good agreement with the experimental results, further indicating that the dimpling process was well captured by the FE model. The increase in the yield stress, tensile strength and maximum load were satisfactorily validated by experimental tests. This is due to the various levels of plastic strain developed throughout the thickness of the steel sheet, resulting in strain hardening. This, in turn, changes the mechanical properties of the steel material and correlated to the increase in strength of the dimpled steel. The cold work applied during the dimpling process and the subsequent mechanical and structural properties were affected by process parameters such as friction and tooth overlapping gap; in which, the overlapping gap had profound effects on the work hardening because plastic strain was developed in a broader region of the whole dimpled sheet.

The FE model reported here enables to achieve a better understanding of the effects of the dimpling process on mechanical and structural properties of dimpled material. The model can be used as an alternative and complementary method to the optimum design of the UltraSTEEL® process and mechanical testing of steel materials and structures.

Acknowledgement

The authors would like to thank the Technology Strategy Board, Hadley Industries plc and the University of Wolverhampton for their supports through a Knowledge Transfer Partnerships project (KTP0077031).

References

[1] Kwon YB, Hancock GJ. Tests of cold-formed channels with local and distortional buckling. Journal of Structural Engineering 1992; 118: 1786–1803.

[2] Lecce M, Rasmussen KJR. Distortional buckling of cold-formed stainless steel sections: experimental investigation. Journal of Structural Engineering 2006; 132: 497–504.

[3] Nguyen VB, Wang CJ, Mynors DJ, English MA, Castellucci MA. Mechanical properties and structural behaviour of cold-rolled formed dimpled steel. Steel Research International 2011; Special Issue: 1072–1077.

[4] Collins J, Castellucci MA, Pillinger I, Hartley P. The influence of tool design on the development of localised regions of plastic deformation in sheet metal formed products to improve structural performance. In: Proceeding of the 10th International Conference on Metal Forming. 2004, paper no. 68.

[5] Letter of conformity BTC 1232LC: Estimating the recommended maximum heights of British Gypsum partitions and linings incorporating various Gypframe metal studs and Gyproc plasterboards. Fire Acoustics Structures, The Building Test Centre, British Gypsum Ltd., 2007.

[6] Nguyen VB, Wang CJ, Mynors, DJ, English MA, Castellucci MA. Compression tests of cold-formed plain and dimpled steel columns. Journal of Constructional Steel Research 2012; 69: 20–29.

[7] Nguyen VB, Wang CJ, Mynors, DJ, English MA, Castellucci MA. Compressive strength tests and design of cold-formed plain and dimpled steel columns. In: Proceeding of the 21st International Specialty Conference on Cold-Formed Steel Structures. 2012, pp.127-142.

[8] Hartley P, Pillinger I. Developments in computational modelling techniques for industrial metal forming process. Proceeding of the Institution of Mechanical Engineers, Part B: Journal of Engineering Manufacture 2001; 215: 903–914.

[9] Nguyen VB, Wang CJ, Mynors DJ, Castellucci MA, English MA. Finite element simulation on mechanical and structural properties of cold-formed dimpled steel. Thin-Walled Structures 2013; 64: 13–22.

[10] Wang CJ, Mynors DJ, English MA. Simulating the UltraSTEEL dimpling process. Key Engineering Materials 2009; 410-411: 449–456.

[11] Sonmez FO, Demir A. Analytical relation between hardness and strain for cold formed parts. Journal of Materials Processing Technology 2007; 186: 163–173.

[12] British Standard, BS EN 10002-1:2001. Metallic materials - Tensile testing - Part 1: Method of test at ambient temperature. 2001.

[13] British Standard, BS 1639:1964. Methods for bend testing of metals. 1964.

[14] Bui QV and Ponthot JP. Numerical simulation of cold roll-forming process. Journal of Materials Processing Technology 2008; 202: 275–282.

Fig. 1

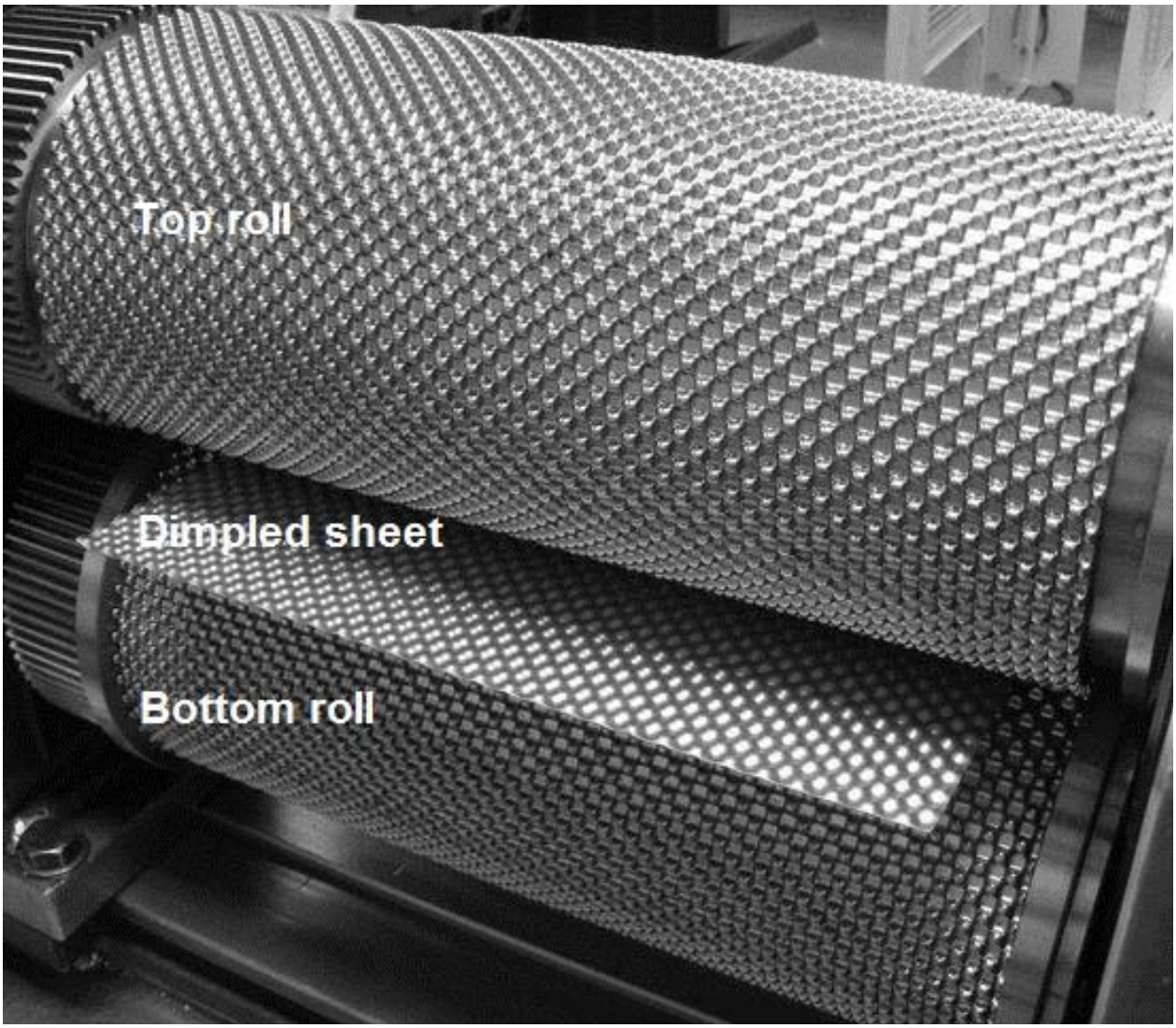

Fig. 2

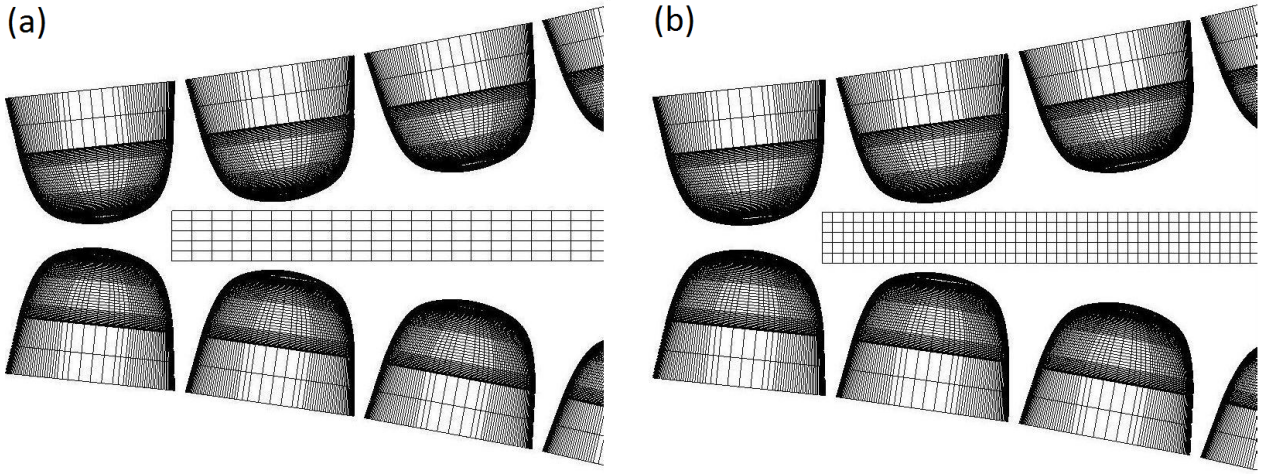

Fig. 3

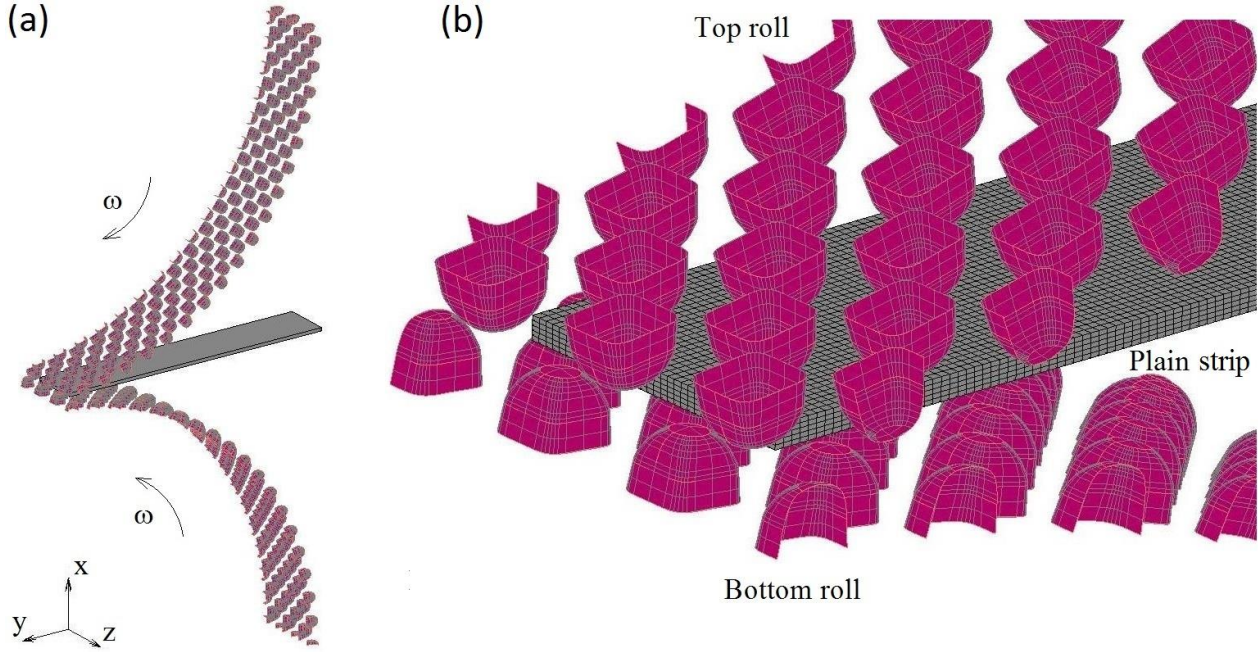

Fig. 4

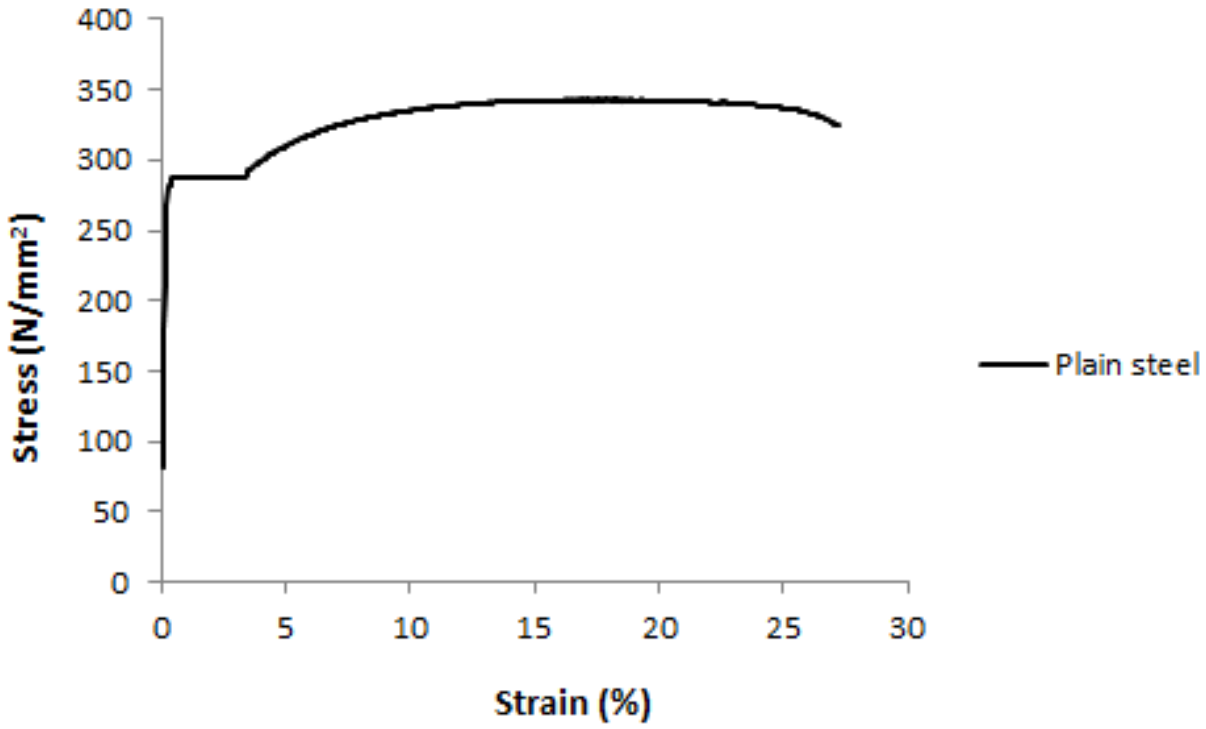
400
350
300
250
200
150
100
50
0
Stress (N/mm²)
0
5
10
15
20
25
30
Strain (%)
Plain steel

Fig. 5

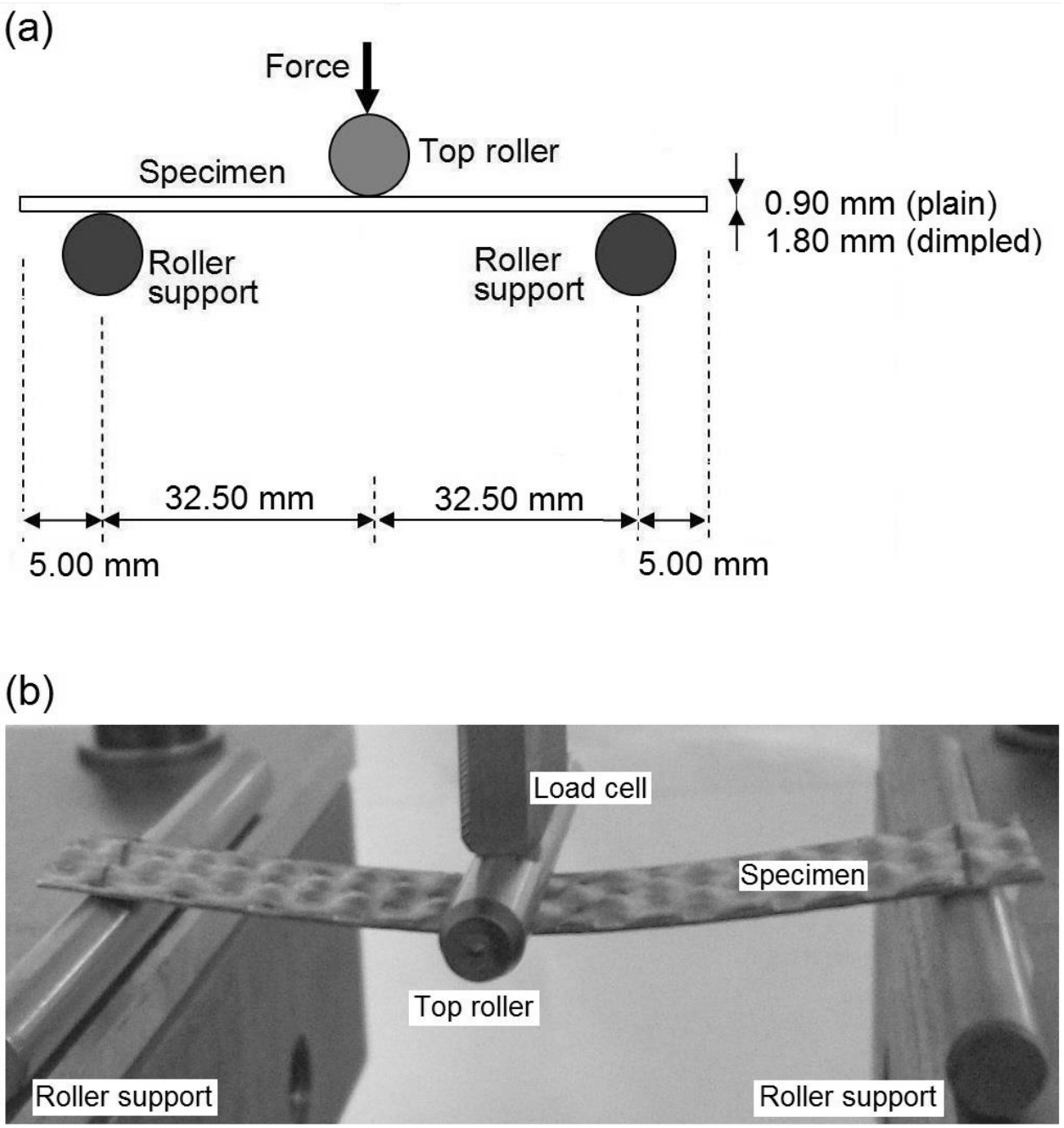
(a)
Force
Top roller
Specimen
0.90 mm (plain)
1.80 mm (dimpled)
Roller support
Roller support
32.50 mm
32.50 mm
5.00 mm
5.00 mm
(b)
Load cell
Specimen
Top roller
Roller support
Roller support

Fig. 6

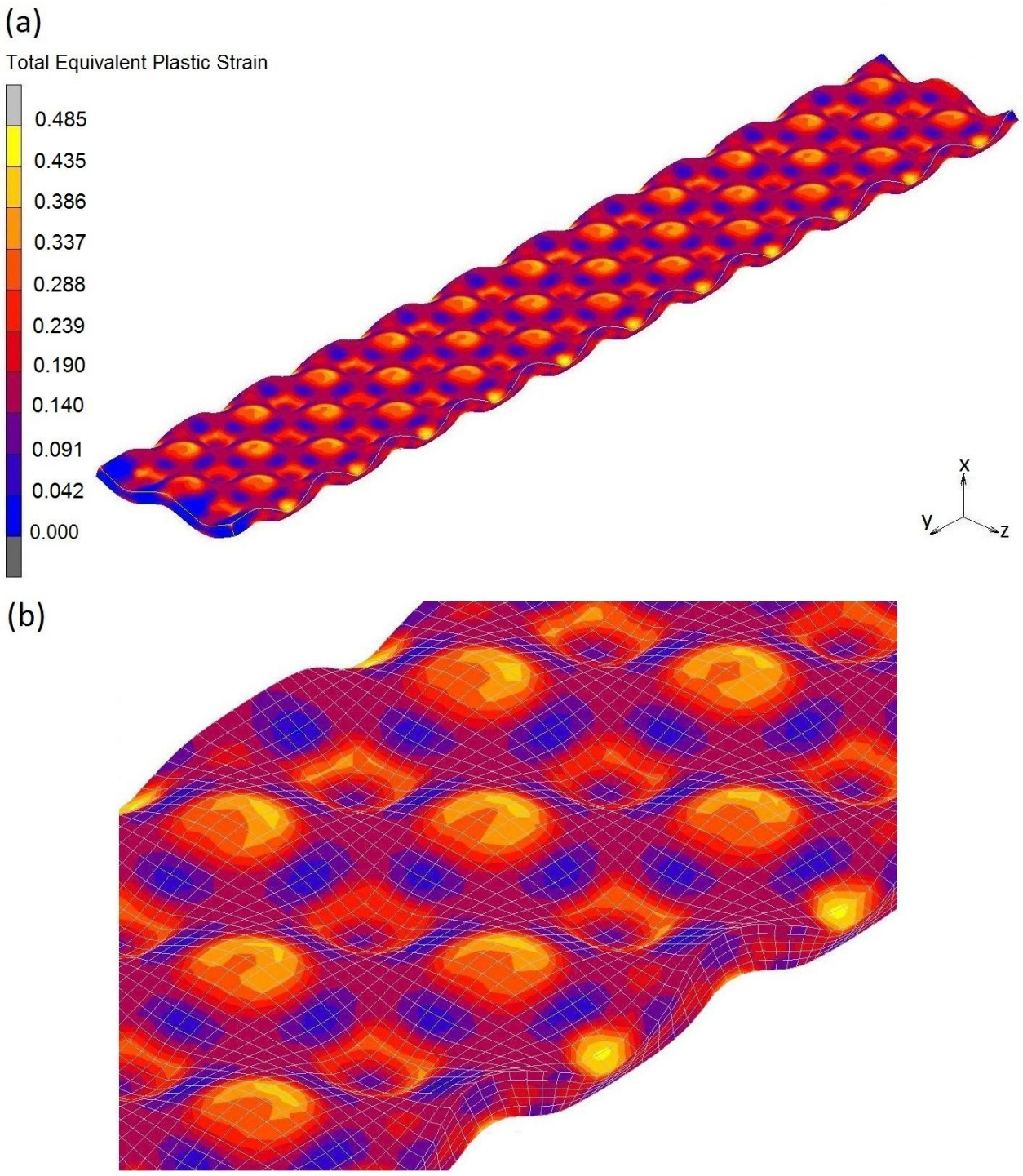
(a)
Total Equivalent Plastic Strain
0.485
0.435
0.386
0.337
0.288
0.239
0.190
0.140
0.091
0.042
0.000
x
y
z
(b)

Fig. 7

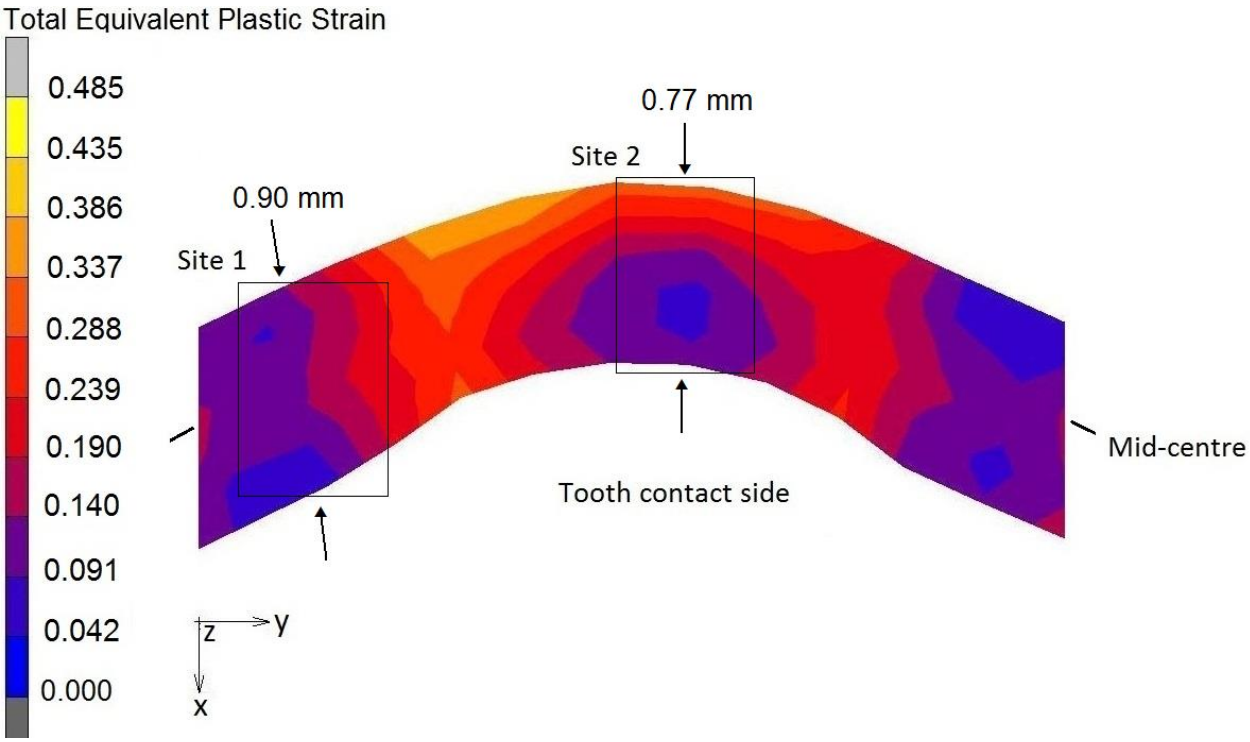
Total Equivalent Plastic Strain
0.485
0.435
0.386
0.337
0.288
0.239
0.190
0.140
0.091
0.042
0.000
0.77 mm
Site 2
0.90 mm
Site 1
Mid-centre
Tooth contact side
z
y
x

Fig. 8

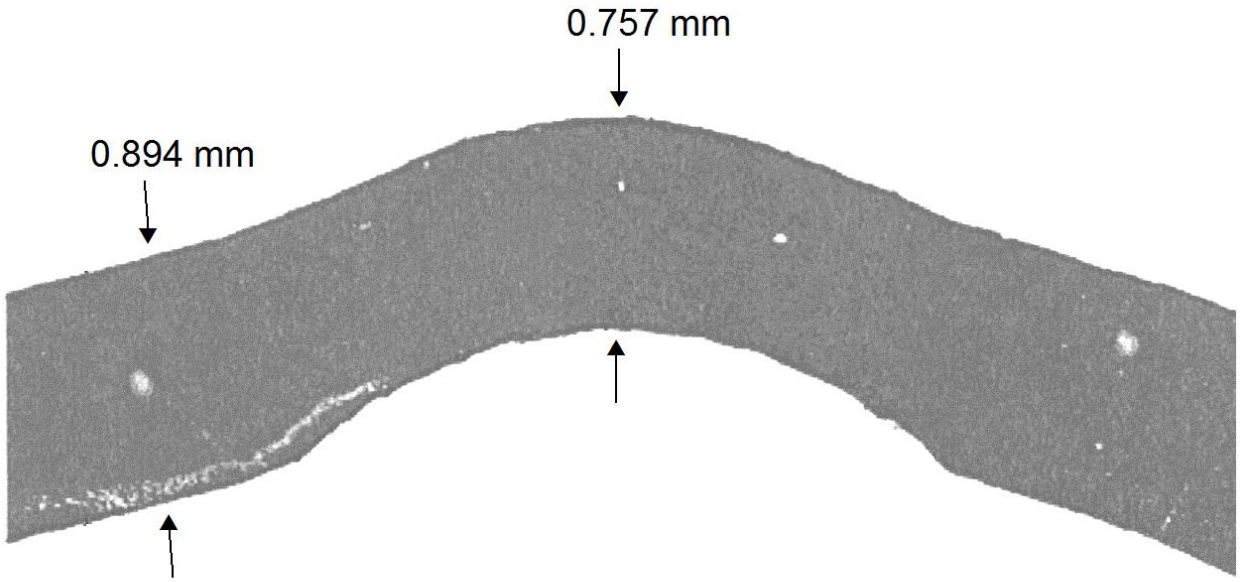
0.757 mm
0.894 mm

Fig. 9

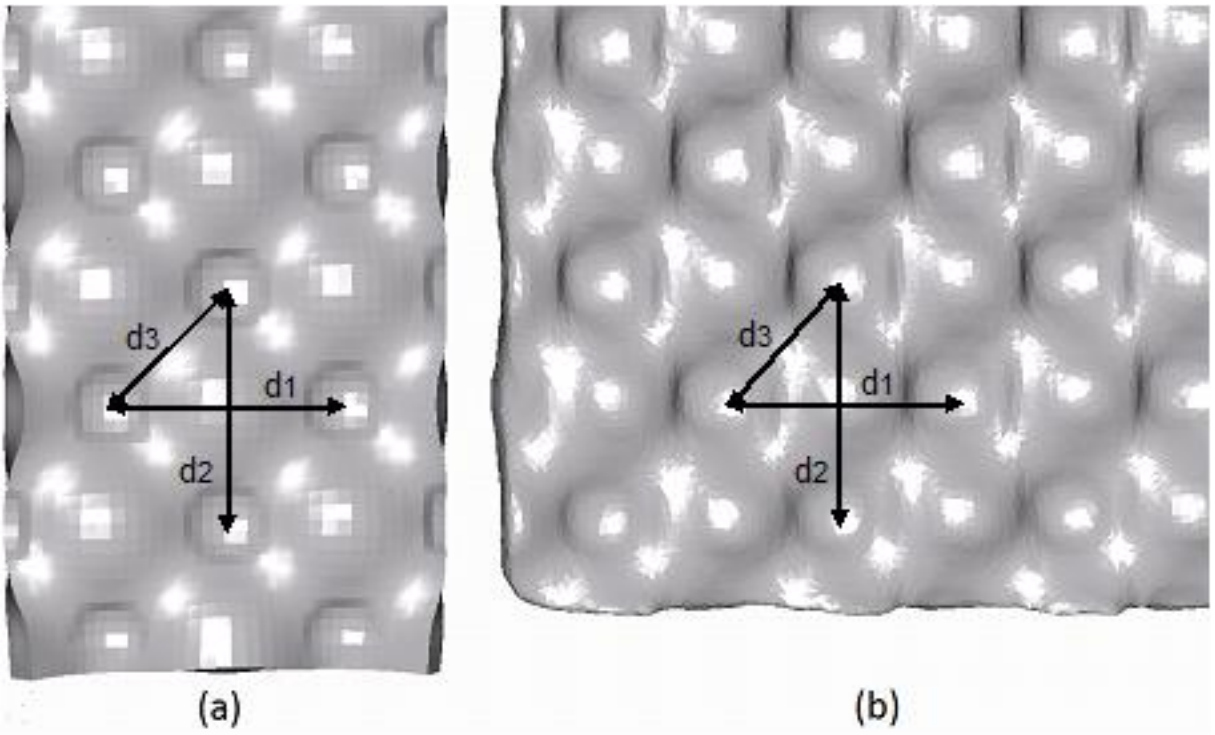
d3
d1
d2
(a)
d3
d1
d2
(b)

Fig. 10

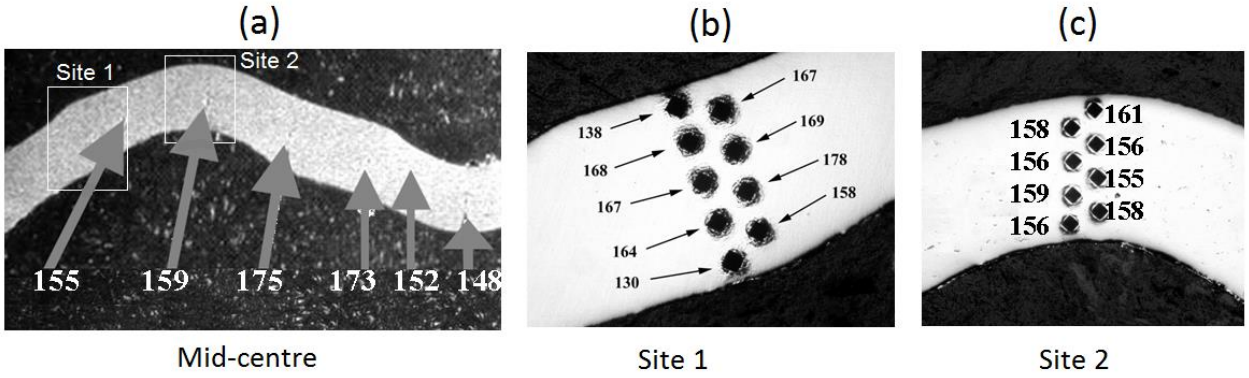
(a)
Site 1
Site 2
155
159
175
173
152
148
Mid-centre
(b)
167
138
169
168
178
167
158
164
130
Site 1
(c)
158
161
156
156
155
159
158
156
Site 2

Fig. 11

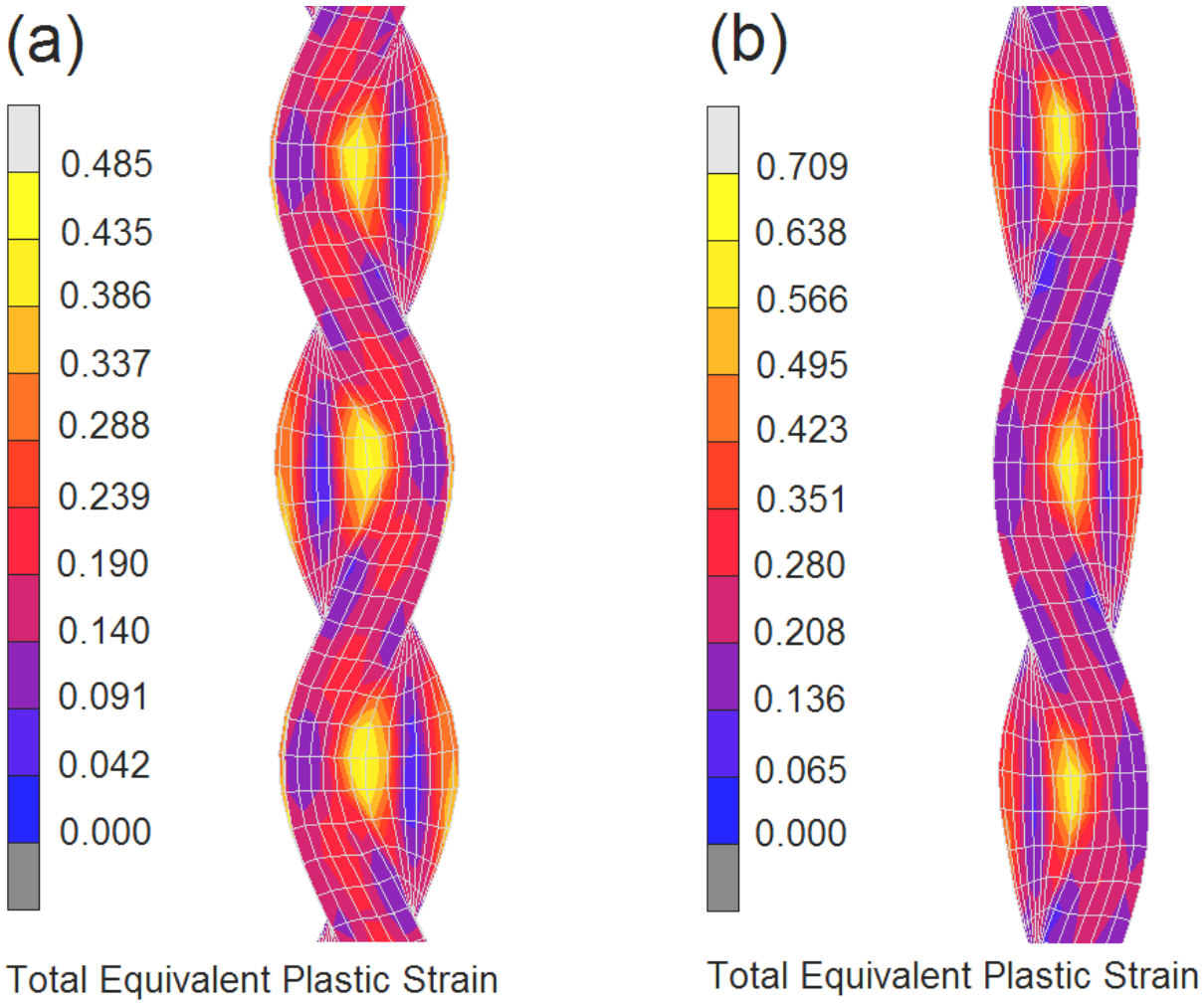
(a)
0.485
0.435
0.386
0.337
0.288
0.239
0.190
0.140
0.091
0.042
0.000
Total Equivalent Plastic Strain
(b)
0.709
0.638
0.566
0.495
0.423
0.351
0.280
0.208
0.136
0.065
0.000
Total Equivalent Plastic Strain

Fig. 12

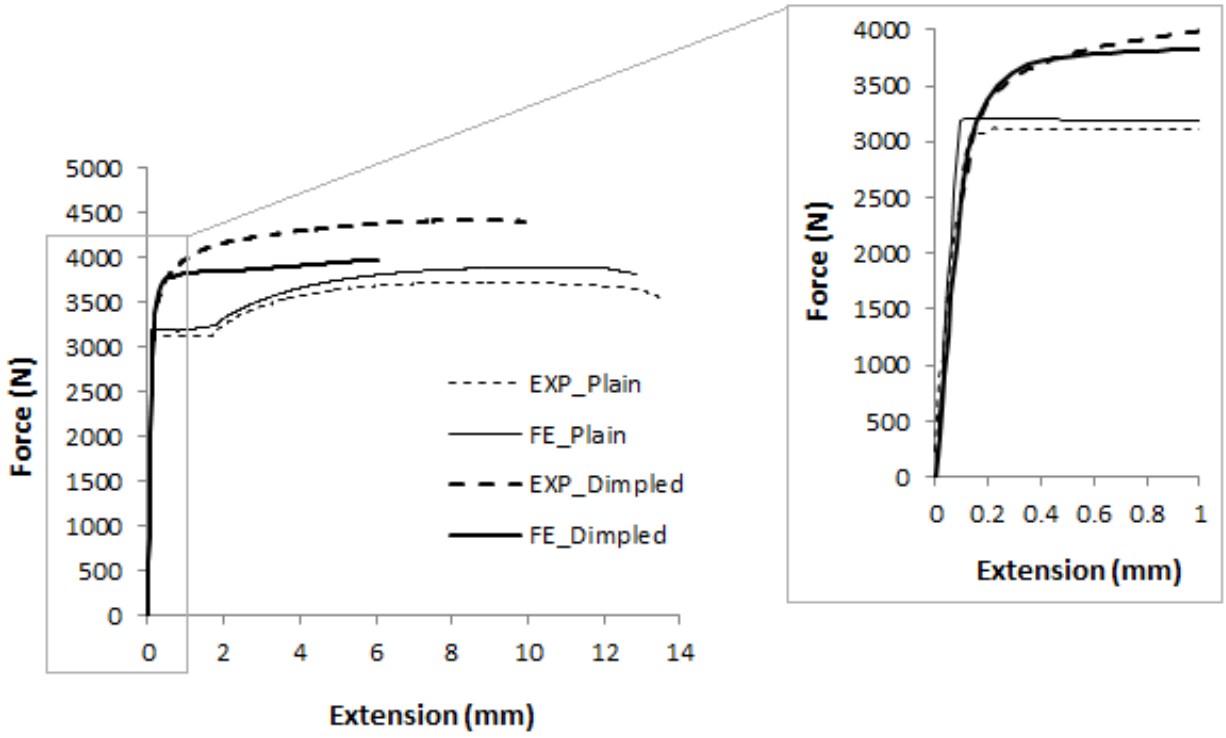
Force (N)
Extension (mm)
EXP_Plain
FE_Plain
EXP_Dimpled
FE_Dimpled
Force (N)
Extension (mm)

Fig. 13

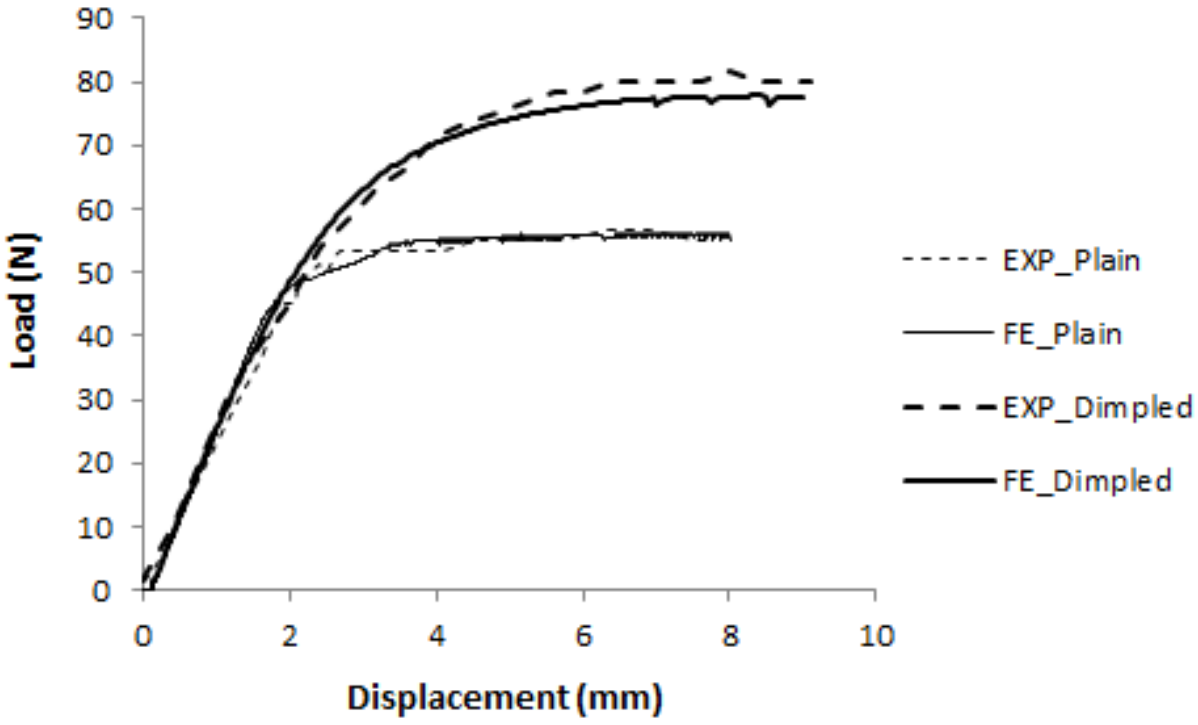
Load (N)
Displacement (mm)
EXP_Plain
FE_Plain
EXP_Dimpled
FE_Dimpled

Fig. 14

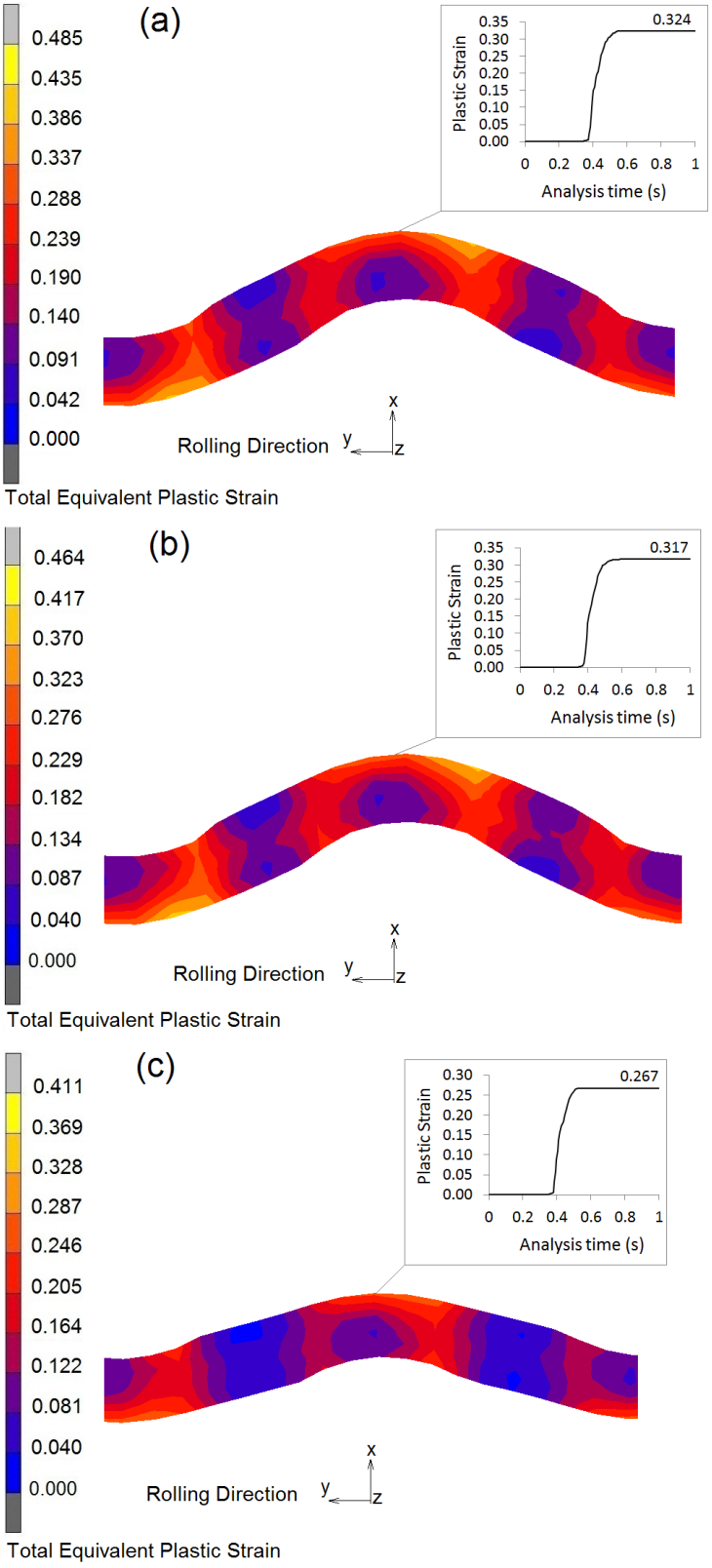
(a)
0.485
0.435
0.386
0.337
0.288
0.239
0.190
0.140
0.091
0.042
0.000
Plastic Strain
0.35
0.30
0.25
0.20
0.15
0.10
0.05
0.00
0.324
0 0.2 0.4 0.6 0.8 1
Analysis time (s)
Rolling Direction
x
y
z
Total Equivalent Plastic Strain
(b)
0.464
0.417
0.370
0.323
0.276
0.229
0.182
0.134
0.087
0.040
0.000
Plastic Strain
0.35
0.30
0.25
0.20
0.15
0.10
0.05
0.00
0.317
0 0.2 0.4 0.6 0.8 1
Analysis time (s)
Rolling Direction
x
y
z
Total Equivalent Plastic Strain
(c)
0.411
0.369
0.328
0.287
0.246
0.205
0.164
0.122
0.081
0.040
0.000
Plastic Strain
0.30
0.25
0.20
0.15
0.10
0.05
0.00
0.267
0 0.2 0.4 0.6 0.8 1
Analysis time (s)
Rolling Direction
x
y
z
Total Equivalent Plastic Strain

Table 1

Analysis no.	Friction coefficient μ	Tooth overlapping gap δ (mm)
1	0.30	0.40
2	0.15	0.40
3	0.30	0.00

Table 2

Analysis no.	Max. Equivalent Plastic Strain	Max. Bending Load (N)
1	0.485	77.9
2	0.464	74.4
3	0.411	72.8